

Article type : Original Article

Cutaneous inflammation differently regulates the expression and function of Angiotensin II types 1 and 2 receptors in rat primary sensory neurons

Sergio Benitez^{1,4}, Alicia Seltzer², Diego Messina¹, Mabel Foscolo¹, Sean Patterson³ and Cristian Acosta^{1*}.

¹Laboratorio de Neurobiología del Dolor. Instituto de Histología y Embriología de Mendoza (IHEM-CONICET), Facultad de Ciencias Médicas, Universidad Nacional de Cuyo, 5500, Mendoza, Argentina.

²Laboratorio de Neurobiología, Instituto de Embriología e Histología (IHEM-CONICET), Facultad de Ciencias Médicas, Universidad Nacional de Cuyo, 5500, Mendoza, Argentina

³Instituto de Fisiología, Facultad de Ciencias Médicas, Universidad Nacional de Cuyo, Mendoza, Argentina; Instituto de Histología y Embriología - CONICET, Universidad Nacional de Cuyo, 5500, Mendoza, Argentina.

⁴Present address: Centro de Biología Integrativa, Facultad de Ciencias, Universidad Mayor, 8580745, Santiago, Chile.

* Corresponding author:

Phone: +54-261-4135000 ext. 2671

e-mail: cacosta@fcm.uncu.edu.ar

ORCID ID: 0000-0001-9333-5843

This article has been accepted for publication and undergone full peer review but has not been through the copyediting, typesetting, pagination and proofreading process, which may lead to differences between this version and the Version of Record. Please cite this article as doi: 10.1111/jnc.14848

This article is protected by copyright. All rights reserved.

Abstract

Neuropathic and inflammatory pain results from cellular and molecular changes in dorsal root ganglion (DRG) neurons. The type-2 receptor for Angiotensin-II (AT2R) has been involved in this type of pain. However, the underlying mechanisms are poorly understood, including the role of the type-1 receptor for Angiotensin-II (AT1R). Here, we used a combination of immunohistochemistry and immunocytochemistry, RT-PCR and *in vitro* and *in vivo* pharmacological manipulation to examine how cutaneous inflammation affected the expression of AT1R and AT2R in subpopulations of rat DRG neurons and studied their impact on inflammation-induced neuritogenesis. We demonstrated that AT2R-neurons express C- or A-neuron markers, primarily IB4, trkA and substance-P. AT1R expression was highest in small neurons and co-localized significantly with AT2R. *In vitro*, an inflammatory soup caused significant elevation of AT2R mRNA while AT1R mRNA levels remained unchanged. *In vivo*, we found a unique pattern of change in the expression of AT1R and AT2R after cutaneous inflammation. AT2R increased in small neurons at 1 day and in medium size neurons at 4 days. Interestingly, cutaneous inflammation increased AT1R levels only in large neurons at 4 days. We found that *in vitro* and *in vivo* AT1R and AT2R acted co-operatively to regulate DRG neurite outgrowth. *In vivo*, AT2R inhibition impacted more on non-peptidergic C-neurons neuritogenesis while AT1R blockade affected primarily peptidergic nerve terminals. Thus, cutaneous-induced inflammation regulated AT1R and AT2R expression and function in different DRG neuronal subpopulations at different times. These findings must be considered when targeting AT1R and AT2R to treat chronic inflammatory pain.

Keywords: AT1 receptor; AT2 receptor; neuritogenesis; inflammatory pain; dorsal root ganglia; nociceptors

Abbreviations

ABC/DAB: avidin-biotin complex/diaminobenzidine

ACE: angiotensin converting enzyme

ARB: angiotensin receptor blocker

AT1R: Angiotensin II type-1 receptor

AT2R: Angiotensin II type-2 receptor

This article is protected by copyright. All rights reserved.

Azil: azilsartan

β -TubIII: beta tubulin III

CFA: complete Freund's adjuvant

CGRP: calcitonin-gene related peptide

DAPI: 4',6'-diamidino-2-phenylindole

DRG: dorsal root ganglion

GDNF: glial-derived neurotrophic factor

HBSS: Hank's balanced salt solution

IB4: isolectin B4

IS: inflammatory soup

Los: losartan

LTM: low threshold mechanoreceptor

MEM: minimum essential medium

NGF: nerve growth factor

PD: PD123319

RRID: research resource identifier (see scicrunch.org)

SP: substance P

Introduction

Acute and chronic/pathological pain of peripheral origin results from changes in the activity of primary afferent neurons. Different neuronal subpopulations within the dorsal root ganglia (DRG) are affected by peripheral inflammation causing lowered nociceptive sensory and electrical thresholds in undamaged fibers (Djoughri *et al.* 2012; Shim *et al.* 2005) as well as spontaneous pain, mechanical allodynia and hyperalgesia (Cook *et al.* 2018; Djoughri *et al.* 2006; Pinho-Ribeiro *et al.* 2017). Recently, the renin-angiotensin system (RAS) has been shown to be involved in normal and pathological sensory function, including inflammation and pain (Ruiz-Ortega *et al.* 2001; Suzuki *et al.* 2003; Bali *et al.* 2014). Angiotensin-II (Ang-

II), which is released during inflammation (Suzuki *et al.* 2003), interacts with both angiotensin type-1 receptor (AT1R) and angiotensin type-2receptor (AT2R) present in the DRG and other peripheral nervous system structures although their role in sensory pathways has yet to be fully understood (Patil *et al.* 2010; Pavel *et al.* 2008; Smith & Muralidharan 2015).

The most widely used antihypertensive drug classes, angiotensin converting enzyme (ACE) inhibitors and Ang-II receptor blockers (ARBs), are used to treat inflammatory diseases through actions independent of their effects on blood pressure (Ranjbar *et al.* 2019). Of notice, AT1R are up-regulated in inflamed tissues. On the other hand, the trend in emerging data supports anti-inflammatory, anti-proliferative and anti-fibrotic roles for AT2Rs, and they also may protect against oxidative stress (Matavelli & Siragy 2015). In fact, it is thought that AT1R and AT2R in general have opposite effects on several cell functions (Chabrashvili *et al.* 2003; Jones *et al.* 2008). However, Ang-II activation of AT2R acting through the NF- κ B pathway led to pro-inflammatory responses (Esteban *et al.* 2004; Wolf *et al.* 2002). These data indicates that the correct functioning of the RAS system demands a complex and finely tuned balance between activation of the two receptors.

The inherent pharmacological consequences of such an integrated mechanism of action are perhaps most clearly seen with Ang-II associated analgesia. Chronic administration of AT1R antagonists has been shown to ameliorate migraine and neuropathic and nociceptive pain (Bali *et al.* 2014; Marques-Lopes *et al.* 2009) whilst selective AT2R antagonists have been proposed as a treatment for chronic inflammatory pain and peripheral neuropathy (Smith & Muralidharan 2015; Smith *et al.* 2013; Shepherd & Mohapatra 2018). It is unclear whether the beneficial effects of RAS blockers in models of neuropathic pain are mediated directly through action on sensory pathways, or indirectly through their attenuating effects on pro-inflammatory mediators.

There is contradictory evidence regarding the nociceptive effect of activating or blocking the AT2R. For instance, a newly identified natural agonist of AT2R, mycolactone, induces analgesia in patients with Buruli ulcers (Marion *et al.* 2014). Both AT2R agonists and antagonists can have an anti-nociceptive effect under different circumstances. Evidently, a deeper knowledge of the mechanisms of action of Ang-II on the inflammatory responses, and on the ability of ARBs to decrease pain perception, would clarify these apparently contradictory results. One such mechanism involves the Ang-II release in response to inflammation (Benigni *et al.* 2010) acting on AT2R to promote neurite outgrowth in cultured cells of neuronal origin (Guimond & Gallo-Payet 2012; Li *et al.* 2005; Namsolleck *et al.* 2013) as well as in cultured adult human DRG neurons (Anand *et al.* 2013; Anand *et al.* 2015;

Chakrabarty *et al.* 2008). In this respect, evidence suggests that structural plasticity of peripheral sensory innervation may play a main role in pain sensation (Cain *et al.* 2001).

Prior observations provided indirect pharmacological evidence for the involvement of AT2R in relieving mechanical allodynia after CFA injection (Chakrabarty *et al.* 2013). However, it is unclear what role AT1R and the interaction between AT1R and AT2R play in inflammatory processes, particularly in identified neuronal subpopulations of DRG neurons as they mediate different sensory modalities. To address this, we carried out a phenotypic characterization of the AT1R and AT2R expressing DRG neurons, and examined how their expression changed in these neuronal subpopulations after induction of cutaneous inflammation. We also looked at Ang-II-induced neuritogenesis in DRG neurons *in vitro* and *in vivo*, and the relative contributions of AT1R and AT2R activation to this process.

Materials and Methods

Animals

We used 3 month old female Wistar rats (RRID:RGD_737929; weight range 175-200g) obtained from Servicio de Animales de Laboratorio, Facultad de Ciencias Veterinarias, Universidad Nacional de La Plata, Argentina) for *in vivo* experiments (initial n=33) and postnatal day 15 (P15, n=15) for primary DRG cell cultures. Animals (3 per cage) were housed in large metallic boxes with wire mesh lids under controlled temperature and humidity with 12h light/darkness cycles and access to food and water *ad libitum*. All experimental procedures were carried out between 9-11 AM. Animals were cared for in accordance with the Guiding Principles in the Care and Use of Animals of the US National Institute of Health. All procedures were approved by the Institutional Animal Care and Use Committee (CICUAL 31/2014 and 102/2017) of the Universidad Nacional de Cuyo, Mendoza, Argentina.

Induction of cutaneous inflammation

Cutaneous inflammation was induced under sevoflurane anesthesia by intradermal injection of 100 μ l Complete Freund's Adjuvant (CFA, Sigma, Cat# F5881) as previously described (Haskins *et al.* 2017). To examine the expression of AT1R and AT2R, DRG were removed after 1 day (CFA1, n=5 rats) and 4 days after CFA (CFA4, n=5 rats). Control rats (n=5) received a single injection of 100 μ l sterile saline solution. Animals were allocated to each experimental group using a random sequence generator (<https://www.random.org/sequences/>). Rats were numbered from 1 to 15, and then assigned to one of 3 groups labeled A, B and C. The software essentially assigned a rat (via its

identifier number) to each group until all had 5 rats each. Notice that a randomized sequence does not contain duplicates (Kim & Shin 2014) . No exclusion criteria were pre-determined and no animals died during the experiments. Because the CFA treatment can cause mild to moderate pain, we observed the behavior of the rats twice a day looking for signs of significant discomfort (like failure to groom etc.). We also weighed them daily and measured their consumption of water and food. Any rats exhibiting a 10% weight loss or a 20% drop in water/food intake would be terminated by humane culling. This, however, was not needed. Analgesia was not provided as most analgesics have anti-inflammatory activity or are opioids, and both will interfere with the aims of the study.

Tissue preparation

After treatment, rats were anesthetized with ketamine (Cat# 01750020010) plus xylazine (Cat# 01750020170, both from Richmond VetPharma) (50 mg/kg & 10 mg/kg) i.p. and transcardially perfused with saline supplemented with heparin (10 UI/ml, Sigma, Cat# H3393) followed by Zamboni's fixative (Stefanini *et al.* 1967). Next skin, L5 DRGs, spinal cord, dorsal root, spinal and sciatic nerve were dissected and post-fixed for 20 min in Zamboni's at RT and dipped in sequentially through graded sucrose solutions (from 10 to 30%) at 4°C. Tissue was frozen and kept at -80°C until used. Serial 7 µm cryostat sections were cut for all tissues except skin (10 µm) and spinal cord (12 µm). Sections were placed on gelatin-coated slides and stored at -20°C for subsequent immunoassays.

Primary antibodies against AT1R and AT2R

We used a goat anti-AT2R from Santa Cruz Biotechnology (Cat# sc-48452, K15, RRID: AB_2225720, 1:200) also used in the DRG by (Anand *et al.* 2013) and other cell types (Dolley-Hitze *et al.* 2010). We chose this antibody because of concerns about the selectivity of other commercially available antibodies against AT2R (Hafko *et al.* 2013). A polyclonal rabbit anti-AT1R (Santa Cruz Biotechnology Cat# sc-579, RRID: AB_2225713, 1:200) was used (Buttler *et al.* 2017). We performed a further characterization of these antibodies comparing them against 2 other commercially available anti-AT2R antibodies (Suppl. Fig. 1). To do this, we ran Western blot analysis and found that AT1R (306) and AT2R (K-15) both detect a single band of the predicted molecular weight in DRGs of 3 different ages and also in the spinal cord (A-B). However, anti-AT2R (H-143) marked a large number of additional bands (C). Next, we examined how the antibodies performed at staining adrenal gland, a known physiological target for Ang-II where the distribution of AT1R and AT2R expression has been reported using non-immune methods. We found that AT1R (306) and AT2R (K-15) but not Alomone's AAR-012 selectively stained the zona glomerulosa and cells within the adrenal

medulla as expected (Johren *et al.* 1995; Macova *et al.* 2008; Pavel *et al.* 2008). We found that AT1R (306) selectively stained motoneurons in the ventral horn of the spinal cord (Pavel *et al.* 2008) while AT2R (K-15) was remarkably more selective than Alomone's AAR-012 staining DRG neurons. K-15 also stained cortical neurons, in agreement with reports using *in situ* hybridization (Lenkei *et al.* 1997).

Other primary antibodies and IB4-binding

We used phenotypic markers of neuronal subpopulations: 1) Staining with isolectin B4 (IB4, Cat# B-1205, RRID:AB_2314661,1:400), which labels small, C- neurons (Fang *et al.* 2006). 2) Mouse anti-NF200 (clone RT97, RRID:AB_528399, DSHB, Iowa University, 1:4000). 3) Rabbit anti-TrkA (Millipore Cat# 06-574, RRID:AB_310180, developed by L. Reichardt; 1:1000). 4) Guinea pig affinity purified anti-Substance P from Neuromics (Cat# GP14110, RRID:AB_2315368, 1:500). 5) Rabbit anti-CGRP (1:2000) characterized by (Gibson *et al.* 1984) and validated by (Lawson *et al.* 1996). A mouse anti- β -tubulin III (β -TubIII) antibody was also used (clone SDL.3D10, Cat# ab11314, RRID:AB_297918, 1:1000). A rabbit anti-PGP9.5 was also used to estimate total neurite length *in vitro* (Cat# RA12103, Neuromics, RRID: AB_2315126, 1:400).

Western blotting

Western Blots were performed as previously described (Acosta *et al.* 2014; Benitez *et al.* 2017) (Suppl. Fig. 1). Total protein was extracted from whole L4/L5 DRGs and spinal cord using Laemmli buffer supplemented with a protease/phosphatase inhibitor cocktail (HALT, Cat# 87786, ThermoFisher). Samples of ~10 μ g of total protein were run on 8% polyacrylamide gels and transferred to PVDF membranes (Cat# GE1060023, Amersham) before blotting. Membranes were blocked with 5% semi-skimmed milk dissolved in tris-buffer saline (TBS) during 1h at RT and then probed overnight with 1:500 polyclonal rabbit anti-AT1R (306) or 1:1000 goat anti-AT2R (K-15) or 1:1000 rabbit anti-AT2R (H-143). We used 1:4000 mouse anti- α -tubulin (eBioscience, Cat# 14-4502-80, RRID:AB_1210457) as loading control. The membranes were washed three times for 5 mins with 0.1% Tween 20 in TBS (TBST) and then blocked again with 5% semi-skimmed milk for 30 min before incubation for 2h at RT with either 1:2000 peroxidase-labeled anti-rabbit (Cat# PI-1000, RRID:AB_2336198) or anti-goat (Cat# PI-9500, RRID:AB_2336124) both from Vector Laboratories. The membranes were washed 3 times for 5 min with TBST and twice for 5 min with TBS. Protein bands were developed using ECLPlus (Amersham) and visualized with the LAS-4000 System (Fujifilm).

Immunohistochemistry

Avidin-biotin complex (ABC/DAB) immunohistochemistry was carried out following previously published protocols (Acosta *et al.* 2014).

Sections were incubated in primary antibody (anti-AT2R 1:200 or anti-AT1R 1:200) diluted in 0.05% Triton X-100 in PBS buffer (PBST) overnight at 4°C. On the following day, sections were incubated with biotinylated horse anti-goat (Cat# BA-9500, RRID:AB_2336123) or anti-mouse (Cat# BA-2001, RRID:AB_2336180) antibodies (1:400) (Vector Laboratories) for 30 min at room temperature. After washings with PBST, sections were incubated 30 min with Streptavidin-HRP (1:200, Cat# S5512, Sigma). To develop the reaction, an ABC standard kit from Vector Laboratories was used (Cat# PK-4000, RRID:AB_2336818). For comparisons between different treatments, all sections were incubated simultaneously for the same length of time.

Double/triple immunofluorescence was conducted as previously described (Benitez *et al.* 2017). Tissues were incubated sequentially in the first primary antibody overnight at 4°C and in secondary antibody appropriate for that primary antibody or IB4 for 2hr at room temperature. Anti- AT2R was used at 1:200, anti-AT1R at 1:200, anti-TrkA at 1:1000, anti-NF200 at 1:4000, anti-Substance P at 1:500, anti- β -TubIII at 1:1000 and anti-CGRP at 1:2000. Secondary antibodies were 1:400 donkey anti-rabbit Alexa-488 (Cat# A32790, RRID:AB_2762833) or Alexa-594 (Cat# A32754, RRID:AB_2762827), goat anti-rabbit Pacific blue (1:100, Cat# P_10994, RRID:AB_2539814), 1:400 goat anti-mouse Alexa-488 (Cat# A_21141, RRID:AB_2535778) or Alexa-594 (Cat# A_21145, RRID:AB_2535781), 1:400 goat anti-guinea pig Alexa-594 (Cat# A_11076, RRID:AB_2534120) and donkey anti-goat Alexa-488 (Cat# A32814, RRID:AB_2762838) or Alexa-594 (Cat# A32758, RRID:AB_2762828), all from Invitrogen. IB4 was conjugated with either FITC or DyLight 594 (1:500, Vector Laboratories, Cat# DL_1207).

Cell cultures

DRGs from all rostrocaudal levels from P15 rats, one per culture, were dissected out following previously detailed protocols (Acosta *et al.* 2014; Acosta *et al.* 2012). We choose this age because a) the neurons have a better survival profile than adult neurons; b) they attached well to a collagen substratum unlike older, adult DRG neurons and c) we have already demonstrated that they express levels of AT2R similar to that of adult DRG (Benitez *et al.* 2017). Briefly, the ganglia were enzymatically digested at 37°C in 0.625% trypsin (Cat# 27250018) for 25 min and then with 0.5% collagenase (Cat# 17100017) for 20 min in HBSS (Hank's Balanced Salt Solution) subsequently quenched with DMEM/F12 (Cat# 11320033) plus 5% fetal bovine serum (Natocor, Argentina) and mechanically dissociated. Isolated cells

were plated onto round coverslips (Bellco Glass, Germany) previously coated with rat tail collagen (300 ng/mm²). Neurons were allowed to attach to the substratum for 3-4 h before addition of DMEM/F12 supplemented with N2 medium (Cat# 17502001) and penicillin/streptomycin (Cat# 15140122). Enzymes, N2 and antibiotic were obtained from GIBCO Thermo Fisher. Non-neuronal cell proliferation was controlled from the start with 10 μM Cytosine β-D-arabinofuranoside (Sigma, Cat# C6645). Cells were kept at 37°C in a 5% CO₂ incubator.

***In vitro* treatment with inflammatory soup**

Three cultures (from 3 rats) were divided in two groups: one group with no trophic factors (NTF) or for 1 day *in vitro* (1DIV) with mouse NGF 7S (10 ng/ml, Cat# 450-01) or rat recombinant GDNF (20 ng/ml, Cat# 450-10) (Peprotech). We chose NGF as AT2R+ and AT1R+ neurons co-localized with trkA (the high affinity receptor for NGF). As most AT2R+ neurons also bound IB4, we tested GDNF, the trophic factor on which IB4+ neurons depend (Dubin & Patapoutian 2010). The other group received in addition an inflammatory soup (IS) containing: 10 μM histamine (Cat# H7125), 10 μM α,β-methylene ATP (Cat# M6517), 1 μM prostaglandin-E2 (Cat# P0409), 1 μM bradykinin (Cat# B3259), 10 μM serotonin (Cat# H9523), 100 nM IL-6 (Cat# I0406), 1 μM TNF-α (Cat# T5944) and 1 μM substance P (Cat# S6883). All drugs obtained from Sigma. These are referred to as NTF+IS, NGF+IS and GDNF+IS.

***In vitro* treatment with Ang-II**

Another 3 cultures (from 3 rats) received daily doses of NGF 7S (10 ng/ml), Ang-II (20 nM, Cat# GPA-100) alone or in combination with AT1R/AT2R selective blockers: 10 nM azilsartan (Cat# A-245) and/or 50 nM PD123319 ditrifluoroacetate (Cat# P-245, all from Alomone Labs, Israel). The cultures were pre-incubated for 15 min at 37°C with the antagonists before addition of Ang-II. Control cultures received neither trophic factors nor Ang-II. Neurons were treated for 2 days (2DIV) to allow measurement of neurite outgrowth.

Semi-quantitative RT-PCR

Specific mRNA levels from 3 cultures with or without IS were determined by RT-PCR as previously described (Kunda *et al.* 2014; Marsh *et al.* 2012; Benitez *et al.* 2017). mRNA was extracted using RNeasy (Cat# 74104, Qiagen). Total mRNA was quantified using a Nanodrop and only samples with an A260:A280 ratio above 1.8 were used. cDNA was synthesized from 200 ng total RNA using the M-MLV kit (Cat# 9PIM170, Promega) supplemented with RNaseOut (Cat# 1077719, Thermo Fisher). AT2R and AT1R mRNA were amplified using Taq polymerase (InbioHighway, Argentina). For AT2R the program

consisted of 2 min at 94°C, 34 cycles of 20 sec at 94°C, 20 sec at 60°C and 45 sec at 72°C, followed by 5 min at 72°C as final extension. For AT1R the program was 3 min at 94°C, 34 cycles of 1 min at 94°C, 1 min at 58°C and 45 sec at 72°C, followed by 15 min at 72°C. β -actin mRNA was used as loading control (32 cycles). We performed a negative control containing RNA instead of cDNA to rule out genomic DNA contamination.

Primers sequences were: AT2R forward: 5'-CAACTTCAGTTTTGCTGCCAC-3'; reverse 5'-CAGGTCCAAAGAGCCAGTCAT-3', predicted product size 335 bp. AT1R forward: 5'-ATCCAAGATGACTGCCCAA-3'; reverse 5'-GCCAAGGCGAGATTGAGAAG-3', predicted product size 179 bp. β -actin forward: 5'-CGGAACCGCTCATTGCC; reverse 5'-ACCCACACTGTGCCCATCTA -3', predicted product size 290 bp. All primers were synthesized by Ruralex (Argentina), custom-designed and checked for specificity using Primer-BLAST. Images of the RT-PCR SYBR Safe (Cat# S33102, Thermo Fisher) stained agarose (Cat# A9539, Sigma) gels were acquired with the LAS-4000 system (Fujifilm) and quantified with ImageJ software (Benitez *et al.* 2017).

Immunocytochemistry

Cultures were removed from the incubator, washed 2 times with PBS and then fixed in 4% PFA (Cat# P6148, Sigma) with 4.2% sucrose (Biopack, Argentina) for 20 min at 4°C, washed again with PBS and permeabilized with 0.2% v/v Triton X-100 (Biopack, Argentina). Non-specific binding sites were blocked by 1 h incubation at room temperature with 5% BSA. Triple immunofluorescence was performed as previously reported (Acosta *et al.* 2014; Acosta *et al.* 2012). Coverslips were incubated sequentially in the first primary antibody overnight at 4°C and then in fluorescent secondary antibody appropriate for that primary antibody for 1 h at room temperature. This cycle was repeated for each primary antibody. Coverslips were mounted with Mowiol 4-88 (Cat# 475904, Merck). Primary antibodies were applied following the sequence: mouse anti- β -TubIII (1:500), goat anti-AT2R (1:200) and rabbit anti-AT1R (1:200). Secondary antibodies were donkey anti-mouse DyLight 549 (1:400, Vector Labs, Cat# A17828), donkey anti-goat DyLight 488 (1:200, Vector Labs, Cat# SA5-10086, RRID:AB_2556666) and goat anti-rabbit Pacific Blue (1:200).

***In vivo* inhibition of Ang-II receptors**

In order to examine the role of AT1R and AT2R on *in vivo* neurogenesis we divided 18 rats in 3 experimental groups (see Fig. 1). Rats were allocated to each experimental group using the same procedure described above (see Induction of cutaneous inflammation) but starting up with 18 numbered rats. One group (n=6) was given oral Losartan (potassium salt, Cozaarex, MSD) dissolved in their drinking water (100 mg/l). The treatment lasted 4 weeks.

The amount of daily drug ingested by each rat was calculated based on the total volume of water drunk divided by the number of rats in each cage. This rendered an effective average dose of losartan of 20 mg/Kg/day. This dosage and length of treatment was used elsewhere to examine numerous physiologically relevant processes (Akershoek *et al.* 2017; Bayar *et al.* 2015; Kamber *et al.* 2015). The second group (n=6) received oral losartan as the first group, but from day 25 to 28 also received a daily i.p. injection of PD 123319 (1mg/Kg/day (Sanchez *et al.* 2008)). Our aim was to assess the effect on neuritogenesis of acutely antagonizing AT2R in rats where AT1R was already suppressed. Control group (n=6) received normal drinking water (NDW). On day 28, cutaneous inflammation was induced in all rats as described above.

Image acquisition and analysis

All analyses were performed as previously detailed in (Acosta *et al.* 2014; Benitez *et al.* 2017) on images captured on a Nikon 80i microscope and the quantification was performed using HCLImage (Hamamatsu, RRID:SCR_015041). For each experimental comparison, 4-6 fields were captured at 40X with identical settings during the same session. All intensity measurements were carried out at the soma as it is assumed that soma levels are similar to those present at the nerve terminals. This quantitative analysis was the only one performed blindly.

AT2R-AT1R intensities measurement: Only neurons with visible nuclei from mid-sections of L5 DRGs were measured. The cross sectional area and mean whole cytoplasmic, edge and inner pixel density were determined for each neuron. We used cytoplasmic levels as indicative of the total available protein including newly synthesized receptors. In the case of the whole cytoplasm, nuclei were excluded. For edge we drew a line (thickness 3 pixels) over the cell perimeter, that likely reflects the amount of the receptor close to or in the plasma membrane). For the perinuclear intensity we also drew a line over the region surrounding the nucleus (from here on inner) (Suppl. Fig. 2). In both cases, the software averages the pixel density (as mean grey) for the entire region under the line. We have used a similar approach to measure membrane-associated (edge) and inner staining for TREK2 (Acosta *et al.* 2014), α 3-Na⁺/K⁺-ATPase (Parekh *et al.* 2010) and HCN1/HCN2 (Acosta *et al.* 2012) in the DRG. The mean pixel densities for each region of the 5 most intensely stained and the 5 least intensely stained neurons in the analyzed section provided 100% and 0% values respectively. All pixel densities were converted to % intensities as described in (Acosta *et al.* 2014; Benitez *et al.* 2017; Haskins *et al.* 2017). Neurons were classed by size: small (those with areas <400 μ m²), medium (400 to 800 μ m²) and large (>800 μ m²) (Lawson 2002). For each antibody/marker, neurons were considered as positive on the basis of

percentage values of neurons that were blindly classed subjectively as clearly stained above background. A subjective score of 1 (visible staining) corresponded to objective AT1R/AT2R values of $\geq 20\%$ above background which were therefore classed as positive.

Neurite length measurement in DRG cell culture: 40X images were captured blindly to avoid biased data acquisition. For image analysis, we drew lines over all visible neurites labeled with β -TubIII and measured their length. Then, for each image, we calculated the neurite length per neuron.

Quantification of nerve terminals in hindpaw skin sections: 10-12 20X randomized images covering most of the section in the epidermal region were captured blindly. Nerve fibers were identified by staining for β -TubIII. CGRP labels peptidergic (likely trkA+) C- and A-fiber neurons while IB4 binds primarily to small unmyelinated C-nociceptor fibers. Due to the fact that IB4 also stains endothelial cells and other non-neuronal cell types (Laitinen 1987), we only quantified as IB4+ nerve terminals those that were also strongly stained for β -TubIII. All visible nerve terminals labeled with β -TubIII/IB4 or β -TubIII/CGRP were sketched and their lengths measured with HCLImage. We also measured the whole area encompassing the epidermis and the dermis, and this value was used to calculate neurite length per area.

Thickness of the epidermis: we measured the thickness of the epidermis (without stratum corneum) in the contralateral and ipsilateral hindpaw of CFA1 rats with or without AT1R and AT2R antagonists (see above). This was done in images taken from 3 serial sections (10 sections in between) of the hindpaw skin per rat, at 20X magnification. The thickness of the dermis was measured using a straight line extending from the basal epithelium of the epidermis to the beginning of the stratum corneum in 10 locations per section (Leiguarda *et al.* 2018).

Hindpaw dorsoventral thickness measurement

Hindpaw dorsoventral thickness was measured by positioning a caliper touching both the ventral and dorsal surfaces of the hindpaw. Care was taken not to compress the hindpaw during measurement.

Statistics

Results are shown as means \pm SEM. The n values are provided in the figure legends. The normality of data was assessed with the D'Agostino-Pearson test. For data sets that failed the normality test, correlations were evaluated using the non-parametric Spearman's test (Spearman's correlation coefficient, r_s , given when significant). Comparisons between multiple treatment groups were performed with Kruskal-Wallis test plus Dunn's multiple comparisons test (Figs. 5B,D; 6A,B, and Suppl. Fig. 3) or with one way ANOVA plus

Tukey's multiple comparisons test (Fig. 7G and Suppl. Fig. 4). Comparisons between two treatments groups were evaluated using Mann-Whitney U test (Figs. 4A-B, 8A-C and Suppl. Fig. 5). All tests were performed with Prism 7 (GraphPad software, RRID:SCR_000306). No sample calculation was performed. We did not conduct any data test for outliers and thus no single data points were excluded. Tests were two-tailed and a level of $p < 0.05$ was considered statistically significant. Significance is indicated on all graphs by * $p < 0.05$, ** $p < 0.01$ and *** $p < 0.001$.

Results

Phenotype of DRG neurons expressing AT2R and AT1R

Small and medium size neurons are strongly stained for AT2R (black arrows, Fig. 2A). Large neurons (asterisks) show little or no staining. Satellite cells show some weak staining. Quantitative image analysis of 251 neurons from L5 mid-sections ($n=5$ rats) showed that AT2R cytoplasmic intensity was significantly and negatively correlated with cell area (Spearman's correlation $r_s = -0.61$, $P < 0.0001$, Fig. 2A). AT2R mean \pm SEM percentages of cytoplasmic staining were similar for small and medium DRG $61.0 \pm 2.2\%$ vs. $54.1 \pm 3.1\%$ respectively with significantly lower levels in large neurons ($6.9 \pm 1.0\%$, $p < 0.001$).

A similar analysis was conducted for AT1R expression in normal L5 DRG. Although sensory neurons of all sizes expressed AT1R, we observed a negative and statistically significant correlation between AT1R cytoplasmic intensities and cell area ($r_s = -0.49$, $p < 0.0001$, Fig. 2B). The mean (\pm SEM) percentage levels of cytoplasmic AT1R differed significantly for small ($61.2 \pm 3.1\%$), medium ($46.5 \pm 2.6\%$) and large ($29.2 \pm 3.0\%$, $p < 0.001$) neurons.

We next examined the co-expression of AT2R and AT1R, as this is of fundamental importance to assess the role of Ang-II on these neurons. White arrows in Fig. 2C indicate AT2R+ neurons that are also AT1R+. Most AT2R+ neurons were also AT1R+ (188 out of 194, 97%) whereas about 80% (188 out of 234) of the AT1R+ neurons were also AT2R+. Thus, the majority of angiotensin-sensitive neurons in the DRG express both receptors.

We next characterized the sensory neuron subpopulation that expressed AT2R. Fig. 2D shows the typical pattern of expression for AT2R, binding of IB4 and trkA. As we reported previously (Benitez et al., 2017) most AT2R+ neurons bind IB4, albeit there are some small and medium sized DRG neurons who exhibit co-localization of AT2R and trkA. Analysis reveals a positive and significant correlation between AT2R and IB4 ($r_s = +0.49$, $p < 0.0001$) but no significant correlation with trkA (Fig. 2E).

We occasionally observed punctate, Golgi-like, low intensity AT2R staining in a few large neurons. To determine which type of myelinated A-neurons they were, we examined the co-localization of AT2R with a marker for myelinated DRG neurons (RT-97) and trkA (as a label for A-nociceptors (Fang *et al.* 2005a)). We found few neurons that evinced at once tenuous AT2R labeling, were trkA+ and had visible RT97 (white arrow in Fig. 2F).

Projections of AT2R+ sensory neurons

We found AT2R staining mostly in laminae I and II of the dorsal horn of the spinal cord, where it co-localizes partially with IB4 (Fig. 3A), and remarkably well with substance P (Fig. 3F). We also observed substantial axonal co-localization of AT2R with IB4 and SP in the L5 dorsal root as well as in the L5 spinal nerve (indicated by white arrows in Figs. 3B-C and G-H). In both cases, some fibers (indicated by arrowheads) were AT2R+ but negative for either IB4 (Fig. 3B-C) or SP (Fig. 3G-H). As expected, AT2R staining co-localized well within a subset of IB4+ fibers in the sciatic and especially in the sural division of the sciatic nerve (indicated with an arrow, Fig. 3D). Finally, free terminals of C-fiber IB4+ neurons in the skin (white arrows) and nerve bundles (asterisk) were AT2R+ (Fig. 3E).

Inflammatory soup up-regulates AT2R but not AT1R *in vitro*

Selective blockade of AT2R with EMA401 reverted mechanical allodynia associated with cutaneous inflammation (Anand *et al.* 2015; Chakrabarty *et al.* 2013). However, the mechanism underlying this effect is poorly understood and so is the possible involvement of AT1R.

Real-time semi-quantitative PCR analysis of 3 separate DRG cultures showed that addition of an IS for 24h caused a significant elevation of AT2R mRNA for all three conditions (NTF vs. NTF+IS $p=0.0014$; NGF vs. NGF+IS $p=0.0018$ and GDNF vs. GDNF+IS $p=0.0315$) (Fig. 4A). We noticed that GDNF alone also caused a significant increase in AT2R mRNA ($p=0.0121$). By contrast, AT1R mRNA levels remained unchanged either by addition of trophic factors or IS (Fig. 4B). This result does not preclude post-transcriptional regulation that could result in altered protein expression, particularly for AT1R. Furthermore, the analysis by PCR does not discriminate between neuronal subpopulations. Thus, it is important to analyse AT1 and AT2 receptor expressions *in vivo*, where the neurons are exposed in a more physiological manner to the inflammatory environment.

CFA cutaneous-induced inflammation regulates AT2R expression

We next examined whether 1- and 4-day CFA-induced cutaneous inflammation altered the expression of AT2R in primary sensory neurons. We measured AT2R staining intensity at 3 locations within each neuron: whole cytoplasm (excluding the nucleus), at the cell edge and at the perinuclear region (called inner). Large neurons exhibited very low and invariant levels of AT2R (see Suppl. Fig. 3). The whole data set, including the measurements done in single neurons, all neuronal sizes and conditions for AT1R and AT2R, plus statistical analyses is presented in Supplementary Tables 1 through 4. Note that the bar plots in figures 5 and 6 show the average %intensity per rat, but the intensity measurements were carried out neuron by neuron.

Representative photomicrographs (Fig. 5A) and detailed quantification (Fig. 5B) revealed that overall AT2R cytoplasmic intensity was unchanged in small and medium size neurons. However, small neurons showed a significant bilateral increment at the cell edge ($55.9 \pm 2.4\%$ for contralateral and $57.2 \pm 1.3\%$ for ipsi) compared to normal ($44.6 \pm 2.7\%$, $p=0.0052$). Mean AT2R intensity also increased significantly ipsilaterally relative to normal and contralateral at the inner region of small neurons (69.6 ± 1.4 vs. 61.5 ± 1.9 vs. 61.2 ± 2.6 , $p=0.0057$). This change in AT2R expression was restricted to small neurons, likely unmyelinated C-neurons.

At CFA4, unlike CFA1, we found a different AT2R expression pattern. First, there was no significant change at any subcellular location in small neurons (Fig. 5C&D). Remarkably, medium size neurons showed statistically significant ipsilateral increments in the average %intensity of AT2R compared to both normal and contralateral at the whole cytoplasm (65.5 ± 1.1 for ipsi vs. 53.6 ± 3.3 for normal vs. 50.2 ± 3.0 for contralateral, $p=0.0021$) and at the cell edge (59.8 ± 1.7 for ipsi vs. 37.3 ± 2.3 for normal vs. 46.1 ± 2.2 , for contralateral, $p<0.0001$). At the perinuclear region (inner) we also observed a significant increment in AT2R mean intensity relative to contralateral (66.4 ± 1.7 , vs. 53.8 ± 3.0 , $p=0.0081$) (Fig. 5D). In summary, our results strongly indicate that AT2R expression increased in small neurons at CFA1 and in medium DRG neurons at CFA4.

CFA cutaneous-induced inflammation regulates AT1R expression

We next studied how cutaneous inflammation affected AT1R expression as its involvement in the peripheral response to inflammation remains unclear.

Fig. 6 summarizes our findings on the expression pattern of AT1R in small, medium and large DRG neurons at CFA1 (A) and CFA4 (B). We observed no changes whatsoever in AT1R mean intensity at CFA1 either at the cytoplasm, the cell edge or inner for any neuronal

subpopulation, except for a modest increment in whole cytoplasm level contralaterally in large neurons (Fig. 6A). Interestingly, at CFA4 we found elevated ipsilateral average %intensity of AT1R in large neurons with no changes in small or medium subpopulations. This increment was statistically significant for ipsilateral vs. normal and contralateral DRG in the cytoplasm (42.7 ± 1.7 vs. 29.6 ± 1.3 for normal and 31.3 ± 2.4 for contralateral, $p=0.004$). Similarly, AT1R levels increased significantly at the cell edge (46.1 ± 2.2 for ipsi vs. 34.5 ± 2.1 for normal and 34.2 ± 2.0 for contralateral, $p=0.0055$). Finally, we found elevated inner AT1R average intensity for ipsilateral compared to normal (42.5 ± 2.8 vs. 29.3 ± 1.2 , $p=0.0007$). Thus, in contrast to the case for AT2R, AT1R expression changed significantly only in large neurons and at CFA4.

***In vitro* neuritogenesis of DRG neurons depends on AT1R and AT2R**

The extent of skin innervation has been linked to pain sensitivity with inflammation leading to an increase in neurite outgrowth. It is also known that inflammation triggers the release of Ang-II and that this molecule induces neuritogenesis in several neuronal types, including primary sensory neurons (Anand *et al.* 2013; Chakrabarty *et al.* 2008; Chakrabarty *et al.* 2013). In light of our observations regarding the expression of AT1R and AT2R after CFA-induced inflammation, we decided to evaluate the roles of these two receptors under controlled conditions with cultured DRG neurons.

To this end, we tested the effect of Ang-II on neurite outgrowth (see Methods). We used NGF 7S as a positive control due to its strong neurite outgrowth promoting activity (Delree *et al.* 1989). Figure 7 (A-F) shows representative confocal micrographs of all experimental conditions with their staining against β -TubIII, AT2R and AT1R plus the mask generated to measure total neurite length in each condition. We stained against AT1R and AT2R to demonstrate that *in vitro* DRG neurons maintain the expression of the receptors and also to exclude the possibility that a lack of effects of Ang-II was due to receptors down-regulation. We did not observe any obvious change in the expression of either AT1R or AT2R. The bar plot in Fig. 7G shows the neurite length per neuron under all conditions. As expected NGF had a strong neurite-promoting activity (411.1 ± 48.7 $\mu\text{m}/\text{neuron}$) compared to NTF (165.5 ± 20.5 $\mu\text{m}/\text{neuron}$, $p<0.0001$). Ang-II also exhibited statistically significant neuritogenic activity compared to NTF (307.3 ± 27.5 $\mu\text{m}/\text{neuron}$, $p<0.0043$) and was not significantly different from NGF. Interestingly, treatment with the AT2R antagonist PD123319 (Ang-II+PD) and azilsartan (a selective competitive inhibitor of AT1R; Ang-II+Azil) resulted in significantly lower average neurite length than with Ang-II alone (154.9 ± 41.8 $\mu\text{m}/\text{neuron}$ for PD and 174.9 ± 25.2 $\mu\text{m}/\text{neuron}$ $p<0.003$ for Azil). This suggests that Ang-II exerted its neuritogenic action via both AT1R and AT2R. Thus, it seems that the individual inhibitors

completely blocked the activity of Ang-II and the combination was below NTF control, although it is not statistically different ($p=0.058$). Note that we obtained the same pattern of neurite outgrowth in the different experimental conditions when measuring neurite length using PGP9.5 instead of β -TubIII (Suppl. Fig. 4), to control for a possible artefact arising from neurite thickness-related staining intensity.

***In vivo* pharmacological manipulation of AT1R and AT2R affects peripheral neurite density**

To determine whether our findings *in vitro* were physiologically meaningful, we looked for an Ang-II effect on neuritogenesis *in vivo*. Of note, one study has already established that antagonizing AT2R with PD123319 affects CFA-induced neuritogenesis (Chakrabarty *et al.* 2013). However, the role of AT1R in this process was not examined. Thus, we evaluated whether selective *in vivo* pharmacological inhibition of AT1R and both AT1R and AT2R altered a) the inflammatory response and b) the neurite density of IB4+ and CGRP+ terminals.

Suppl. Fig. 5A shows the induction of edema at CFA1 in the ipsilateral (CI) vs. contralateral (CC) hindpaw. Losartan failed to reduce or prevent the formation of this edema (Los I vs. Los C) and so did the combination of 4 weeks losartan plus 3 days PD123319 (Los+PD I vs. Los+PD C). Another marker of inflammation is the thickness of the epidermal layer, which increases after CFA treatment (Leiguarda *et al.* 2018). At CFA1, we found that the mean epidermal thickness increased ipsilaterally under all experimental conditions (Suppl. Fig. 5B). This confirms our finding that neither chronic low dose losartan nor the combination of losartan plus PD at the concentrations we used was effective in reducing or preventing edema. We also observed thickened epidermal layer in the contralateral side of losartan-treated rats compared to control. This may be due to the ability of losartan to induce significant elevation in circulating levels of the growth factors receptors EGFR and KGFR (Koga *et al.* 2008).

Because previous reports showed apparent no change in neurite outgrowth with CFA but lacked proper quantification (Chakrabarty *et al.* 2013) we studied the effect of Los and Los+PD on the neurite density of myelinated terminals. We found that the density of myelinated terminals increased significantly after CFA in control rats ($p=0.0151$). This increment was not prevented by Los ($p=0.0041$) but was suppressed by Los+PD (Fig. 8A).

We also examined the impact of the treatments in IB4+ free terminals (Fig. 8B). As expected, control rats exhibited a marked increment in the density of IB4+ neurites ipsilaterally at CFA1 ($p=0.017$). Rats treated with Losartan showed no ipsilateral increment

in neurite density compared to the contralateral side. These rats also exhibited a much lower level of neuritogenesis than control rats (CI vs. Los I, $p=0.007$). Although there was no statistically significant reduction in IB4+ neurite density contralaterally, the trend was for these animals to exhibit less neuritogenesis than control rats. Surprisingly, the co-administration of PD123319 with Los resulted in a drastic reduction of IB4+ neurite density contralaterally compared to control ($p=0.003$). This treatment also resulted in very low levels of innervation ipsilaterally, although CFA still caused a significant increment when compared to the contralateral foot. Our findings indicate that simultaneously blocking AT1 and AT2 receptors has a systemic, bilateral arresting effect on neuritogenesis of IB4+ C-neurons.

Finally, we found that Losartan treatment abolished the ipsilateral up-regulation of peptidergic fibers neuritogenesis induced by CFA (there was no difference between Los C vs. Los I). The addition of PD did not change this effect ($p=0.0519$) (Fig. 8C). Therefore, it seems that in the case of peptidergic terminals signaling of Ang-II through AT1R is dominant over AT2R.

Discussion

Here we show a full phenotypic characterization of primary sensory neurons that express AT2R. We also demonstrate a unique change in the pattern of expression of AT1R and AT2R in different neuronal subpopulations at different times in response to cutaneous inflammation. We provide the first demonstration of a direct regulation of AT2R *in vitro* by an inflammatory soup and also evidence that GDNF could up-regulate this receptor. We establish the co-localization of AT1R and AT2R and examined in detail their interplay as mediators of Ang-II induced neurite outgrowth *in vitro*. We found selective effects of Ang-II on *in vivo* neuritogenesis of non-peptidergic C-fiber neurons, CGRP+ nerve terminals and also myelinated fibers by pharmacologically manipulating AT1R and AT2R. Taken together, our data indicate that in the DRG neurons exposed to inflammation, AT1R and AT2R act cooperatively instead of antagonizing each other, as it is the canonical view.

Our phenotypic multifaceted characterization using antibodies and pharmacological tools confirms and expands previous published results showing the presence of AT2R at sites where its activation could lead to the regulation of nociception (Anand *et al.* 2013; Benitez *et al.* 2017; Chakrabarty *et al.* 2013). Note that the use of commercially available antibodies has some limitations (Goodman 2018). The specificity of the antibodies against AT2R and AT1R has been questioned (Hafko *et al.* 2013). Thus, we carried out a validation of the

antibodies used in this study (Suppl. Fig. 1). Nonetheless, we acknowledge that the results coming from their use must be interpreted with caution.

Our data show that AT2R is preferentially expressed in non-peptidergic (IB4-binding) likely C-nociceptors in line with our previous study (Benitez *et al.* 2017). The receptor was also present in peptidergic (trkA+/SP+) neurons that encompass both small C-nociceptors and also medium size A-neurons (Fang *et al.* 2005a). The latter include the type II A-mechanoheat units with moderate conduction velocities and higher mechanical and lower heat thresholds (Djoughri & Lawson 2004). Low levels of AT2R in a few trkA+/RT97+ large neurons may indicate that the receptor was also present in A β -nociceptors. These neurons are high-threshold mechanoreceptors thought to represent ~20% of all A α/β neurons in the DRG (Dubin & Patapoutian 2010; Fang *et al.* 2005b).

We found that AT1R in all neuronal sizes, although its expression was highest in small neurons, in agreement with previous studies (Pavel *et al.* 2008; Patil *et al.* 2010). The fact that AT1R and AT2R are often present in the same neurons warranted examination of their possible interplay in the context of cutaneous inflammation. Our first observation showed that exposure of purified DRG cultures to a complex inflammatory soup for 24h caused an increment in the mRNA levels of AT2R but not of AT1R. This suggested that a similar mechanism might be operating during chronic cutaneous inflammation.

It is interesting to note that GDNF and its high affinity receptor GDFR α 1/Ret in IB4+ neurons are involved in hyperalgesic priming (Joseph & Levine 2010) and also in persistent muscle pain (Alvarez *et al.* 2012). We found that GDNF stimulates AT2R mRNA synthesis in DRG cultures, an observation that agrees with the known GDNF-dependence of survival and phenotypic differentiation of IB4-binding neurons (Zwick *et al.* 2002).

Our finding that CFA1 increased AT2R expression in small, C-like neurons while CFA4 increased the receptor expression in medium A-neurons indicates that AT2R is selectively and differentially modulated throughout the inflammation process. To our knowledge, this is the first time this unique pattern has been reported. Our observed simultaneous increment in AT2R at the inner and edge probably indicates enhanced synthesis *de novo* plus transport towards the membrane. This aspect of the change in expression requires further examination but agrees with studies showing that enhanced membrane trafficking of pain-facilitating molecules underlies the response to inflammation and nerve damage (reviewed by (Ma & Quirion 2014)).

In contrast to the pattern seen with AT2R, AT1R expression remained largely unchanged in all cell sizes and subcellular locations at CFA1 but increased significantly in large neurons at

CFA4. To put this surprising finding in context, other researchers found that in a model of CCI the administration of Ang-II led to an increase in the number of large ATF3+ neurons (a marker of neuronal damage). This effect was reverted by treatment with losartan but not with PD123319 (Pavel *et al.* 2013). Also, there is evidence that selective activation of non-nociceptive A β neurons can induce neuropathic pain (Tashima *et al.* 2018). Thus, there is a possible functional link between likely A α / β low-threshold mechanoreceptors or may be A β -nociceptors and AT1R, but the underlying mechanism and its physiological meaning remains unclear. One possible interpretation for this unique pattern of change in the expressions of AT1R and AT2R is that AT2R predominantly expressed in small likely C-fiber neurons is initially recruited by the inflammation, producing primary mechanical and heat hyperalgesia as part of the nocifensive response to the insult. At 4 days after CFA, the inflammation can then recruit large neurons carrying AT1R. This second phase is associated with the adaptive response to inflammatory pain, and often involves A-fiber like non-nociceptive neurons.

Chronic inflammation is associated with pathological pain. One mechanism proposed to underlie this connection is that pro-inflammatory mediators promote neuritogenesis of both peptidergic and non-peptidergic nociceptors and possibly their sensitization (Anand *et al.* 2013). This hyper-innervation has been shown in skin (reviewed in (Hendrix & Peters 2007)) and in a model of vestibulodynia (Chakrabarty *et al.* 2018; Sharma *et al.* 2018). Thus, we decided to examine the impact of Ang-II on DRG neurite outgrowth, first *in vitro* and then *in vivo*. In our *in vitro* assays to examine neuritogenesis we found that both AT2R and AT1R stimulates neurite outgrowth. This agrees with a previous report that Ang-II enhanced neurite outgrowth in cultured DRG neurons, an effect that was prevented by treatment with an AT2R antagonist (Anand *et al.* 2013). A similar role for this receptor was seen in CFA-induced vestibulodynia where disruption of the RAS system and antagonism of AT2R attenuated neuritogenesis (Chakrabarty *et al.* 2018; Sharma *et al.* 2018). Note that CFA-induced cutaneous inflammation triggers an elevation in the local levels of renin and angiotensinogen, which are released by T-cells and macrophages, recruited to the site of inflammation (Chakrabarty *et al.* 2018; Chakrabarty *et al.* 2013). Additionally, recent evidence shows that macrophages express AT2R which upon activation by Ang-II release reactive oxygen/nitrogen species. These alter the function of TRPA1 receptors in sensory neurons (Shepherd *et al.* 2018). Thus, macrophages recruited early during cutaneous inflammation may contribute to inflammatory pain via potentiation of the local renin-angiotensin system and also by sensitizing TRPA1+ terminals.

Ang-II was reported to promote neurite growth in hypothalamic neurons through AT1R (Yang *et al.* 2002) although ours is the first report of the involvement of this receptor in DRG neurogenesis. Conversely the AT1R antagonist olmesartan promoted neurite outgrowth in cultured fetal ventral spinal cord explants and protected spinal motor neurons *in vivo* after partial axotomy of the sciatic nerve (Iwasaki *et al.* 2002). Thus, there is an open question as to what signal causes AT1R to act neurogenic. The observation that activation of AT2R improves the growth of neurites of cultured corticospinal neurons (Namsolleck *et al.* 2013), may provide a solution to this conundrum if the effect of olmesartan is simply to free AT2R to act as neurogenic. In other words, AT1R may act as a constitutive brake on the neurogenic activity of Ang-II. In support of this interpretation, in NG108-15 cells expressing both AT1R and AT2R Ang-II caused neurite retraction, while in those expressing AT2R alone it promoted neurite outgrowth (Laflamme *et al.* 1996). However, this does not appear to be the case in DRG neurons, as most of them co-express both receptors and respond to activation of either receptor by promoting neurite outgrowth. Nonetheless, experimental evidence demonstrates a cross-talk between the two receptors, an aspect linked to the differentiation state of cells.

Our observation that *in vivo* chronic losartan failed to impair the inflammation-induced increment in myelinated terminals while adding the AT2R blockade succeeded, suggests that there was a subpopulation of large AT1R+ neurons whose neurogenesis was independent of Ang-II. However, the fact that blocking both receptors prevented CFA-induced neurite growth of these neurons suggests the existence of a paracrine control mechanism involving AT2R. We speculate that an unknown factor released by AT2R+ neurons (different from Ang-II) may be controlling the neurogenesis in these large myelinated neurons. An alternative interpretation is that the subpopulations that respond to inflammation are the A δ and A β -nociceptors which would be affected by dual receptor blockade but not by AT1R blockade alone, as the neurite outgrowth in large neurons appears to be Ang-II independent.

Here we provide the first demonstration that IB4+ C-fiber cutaneous innervation depends (at least partially) on recruiting AT1R and AT2R upon CFA-induced release of Ang-II. As IB4+ neurons mediate mechanical and heat hyperalgesia in the rat (Cavanaugh *et al.* 2009; Tarpley *et al.* 2004) any significant alteration in their nerve endings (length, reach and branching) might affect their ability to respond to noxious stimuli. This agrees well with previous reports indicating that antagonizing AT2R with EMA401 reduced mechanical allodynia in a rat model of CFA (Anand *et al.* 2015) and also proved efficacious in the treatment of post-herpetic neuralgia in a limited clinical trial (Rice *et al.* 2014). However, no

previous studies have associated AT1R with neurite outgrowth of IB4+ neurons. One report showed that blockade of the AT1 receptor with losartan in a rat model of CCI prevented tactile hyperalgesia and attenuated cold hyperalgesia, but failed to affect the response to noxious heat stimulus (Pavel *et al.* 2013). Thus, we propose that a reduction in the neurite length of IB4+ neurons may underlie this effect. One unexpected result was the significant reduction in contralateral IB4+ neurites with the dual blockade. This might result from a more substantial systemic effect on the contralateral side, while other neurite-promoting molecules (RAS-independent) are active ipsilaterally.

Regarding peptidergic nerve endings (these include C, A δ and some A β trkA+ nociceptors) we found that AT1R blockade abolished the ipsilateral up-regulation of neuritogenesis induced by CFA. Surprisingly, addition of AT2R blockade did not modify this effect. Note that treatment with PD123319 alone in CFA-treated rats showed that AT2R is involved in CGRP-like long-term hyperinnervation of the skin (Chakrabarty *et al.* 2013). However, unlike our study, these authors did not examine either the effect of blocking AT1R alone or both receptors. Thus, it is possible that the discrepancy between our findings and theirs is due to the interplay between the receptors.

Additionally, as we performed the *in vitro* studies in P15 DRG neurons and the *in vivo* pharmacology in P90 rats, discrepancy in the results might be expected reflecting age-related differences in physiology. However, what we observed *in vivo* confirms what we found *in vitro*.

Accumulating evidence suggests that regulation of mutually antagonistic AT1R and AT2R is essential for maintaining control of inflammation and that an imbalance between these two receptors is potentially pathological (Smith & Missailidis 2004). Most papers in the literature have focused on either AT1R or AT2R but it is important to remember that any C- or A-fiber neuron exposed to Ang-II will have both receptors activated simultaneously. Depending on the relative levels of the two receptors (variable amongst neuronal subpopulations and pathologies) and how they affect each other the net outcome of their activation can be very different. Thus, the key may lie in the balance between the level of expression and activity of the two receptors. Using an experimental paradigm similar to ours, (Hashikawa-Hobara *et al.* 2012) showed that administration of the AT1R blocker candesartan improved Ang-II pro-neuritogenic activity mediated via AT2R.

In conclusion, ARBs have recently been promoted as potential drugs to alleviate chronic pathological pain associated with nerve injury and inflammation. However, most studies have underplayed the potential cross-talk between AT1R and AT2R. This would be

particularly relevant for patients using anti-hypertensive regimes based on ARBs (mostly AT1R antagonists) who rely on AT2R antagonists as a palliative for pain. Given the range of neuronal subpopulations expressing AT1R and AT2R, their co-localization in these neurons and their significant interplay, it might be beneficial to examine mechanoperception and proprioception and the presence of paresthesia/dysesthesia in these patients.

--Human subjects --

Involves human subjects:

If yes: Informed consent & ethics approval achieved:

=> if yes, please ensure that the info "Informed consent was achieved for all subjects, and the experiments were approved by the local ethics committee." is included in the Methods.

ARRIVE guidelines have been followed:

Yes

=> if it is a Review or Editorial, skip complete sentence => if No, include a statement: "ARRIVE guidelines were not followed for the following reason:
"

(edit phrasing to form a complete sentence as necessary).

=> if Yes, insert "All experiments were conducted in compliance with the ARRIVE guidelines." unless it is a Review or Editorial

Acknowledgements

We thank Dr. Patricia Kunda and Prof. Sally Lawson for helpful comments on the manuscript.

Author contributions

Designed experiments and analyzed data: SB, AS, DM, SP, CA; performed experiments: SB, DM, MF, CA; provided essential reagents and promoted the study: AS, SP; wrote the manuscript: SB, AS, DM, SP, CA; conceived and managed the study: AS, CA.

Funding

SB was supported by a post-doctoral fellowship from the National Research Council of Argentina (CONICET). DM has a doctoral fellowship from CONICET. MF holds a position as Principal Technician in the IHEM and is a career member of CONICET. AS, SP and CA are researchers from CONICET (Argentina). This work has been funded by Fondo Nacional para la Ciencia y la Tecnología (FONCyT-ANPCyT PICT-2014-0651 to CA) and by the Programa I + D, Secretaría Ciencia, Técnica y Posgrado, Universidad Nacional de Cuyo, 06/P28 Res-571/2015 to CA and AS.

Compliance with ethical standards

Animals used in this study were cared for in accordance with the Guiding Principles in the Care and Use of Animals of the US National Institute of Health. All procedures were approved by the Institutional Animal Care and Use Committee (CICUAL 31/2014 and 102/2017) of the Universidad Nacional de Cuyo, Mendoza, Argentina.

Conflict of interest

The authors declare no competing financial interest.

Open Science Badges

This article has received a badge for ***Open Materials*** because it provided all relevant information to reproduce the study in the manuscript. The complete Open Science Disclosure form for this article can be found at the end of the article. More information about the Open Practices badges can be found at <https://cos.io/our-services/open-science-badges/>.

References

- Acosta, C., Djouhri, L., Watkins, R., Berry, C., Bromage, K. and Lawson, S. N. (2014) TREK2 expressed selectively in IB4-binding C-fiber nociceptors hyperpolarizes their membrane potentials and limits spontaneous pain. *J Neurosci* **34**, 1494-1509.
- Acosta, C., McMullan, S., Djouhri, L., Gao, L., Watkins, R., Berry, C., Dempsey, K. and Lawson, S. N. (2012) HCN1 and HCN2 in Rat DRG neurons: levels in nociceptors and non-nociceptors, NT3-dependence and influence of CFA-induced skin inflammation on HCN2 and NT3 expression. *PLoS One* **7**, e50442.
- Akershoek, J. J., Brouwer, K. M., Vlig, M., Boekema, B., Beelen, R. H. J., Middelkoop, E. and Ulrich, M. M. W. (2017) Differential effects of Losartan and Atorvastatin in partial and full thickness burn wounds. *PLoS One* **12**, e0179350.
- Alvarez, P., Chen, X., Bogen, O., Green, P. G. and Levine, J. D. (2012) IB4(+) nociceptors mediate persistent muscle pain induced by GDNF. *J Neurophysiol* **108**, 2545-2553.
- Anand, U., Facer, P., Yiangou, Y., Sinisi, M., Fox, M., McCarthy, T., Bountra, C., Korchev, Y. E. and Anand, P. (2013) Angiotensin II type 2 receptor (AT2 R) localization and antagonist-mediated inhibition of capsaicin responses and neurite outgrowth in human and rat sensory neurons. *Eur J Pain* **17**, 1012-1026.
- Anand, U., Yiangou, Y., Sinisi, M. et al. (2015) Mechanisms underlying clinical efficacy of Angiotensin II type 2 receptor (AT2R) antagonist EMA401 in neuropathic pain: clinical tissue and in vitro studies. *Mol Pain* **11**, 38.
- Bali, A., Singh, N. and Jaggi, A. S. (2014) Renin-angiotensin system in pain: existing in a double life? *J Renin Angiotensin Aldosterone Syst* **15**, 329-340.
- Bayar, A., Turan, A., Gulle, K., Akpolat, M., Turan, I. and Turhan, E. (2015) The Effects of the Angiotensin Converting Enzyme Inhibitor Enalapril and the Angiotensin II Type 1 Receptor Blocker Losartan on Fracture Healing in Rats. *Clin Invest Med* **38**, E164-172.
- Benigni, A., Cassis, P. and Remuzzi, G. (2010) Angiotensin II revisited: new roles in inflammation, immunology and aging. *EMBO Mol Med* **2**, 247-257.

- Benitez, S., Seltzer, A. and Acosta, C. (2017) Nociceptor-like rat dorsal root ganglion neurons express the angiotensin-II AT2 receptor throughout development. *Int J Dev Neurosci* **56**, 10-17.
- Buttler, L., Jordao, M. T., Fragas, M. G., Ruggeri, A., Ceroni, A. and Michelini, L. C. (2017) Maintenance of Blood-Brain Barrier Integrity in Hypertension: A Novel Benefit of Exercise Training for Autonomic Control. *Front Physiol* **8**, 1048.
- Cain, D. M., Wacnik, P. W., Turner, M., Wendelschafer-Crabb, G., Kennedy, W. R., Wilcox, G. L. and Simone, D. A. (2001) Functional interactions between tumor and peripheral nerve: changes in excitability and morphology of primary afferent fibers in a murine model of cancer pain. *J Neurosci* **21**, 9367-9376.
- Cavanaugh, D. J., Lee, H., Lo, L., Shields, S. D., Zylka, M. J., Basbaum, A. I. and Anderson, D. J. (2009) Distinct subsets of unmyelinated primary sensory fibers mediate behavioral responses to noxious thermal and mechanical stimuli. *Proc Natl Acad Sci U S A* **106**, 9075-9080.
- Cook, A. D., Christensen, A. D., Tewari, D., McMahon, S. B. and Hamilton, J. A. (2018) Immune Cytokines and Their Receptors in Inflammatory Pain. *Trends Immunol* **39**, 240-255.
- Chabrashvili, T., Kitiyakara, C., Blau, J., Karber, A., Aslam, S., Welch, W. J. and Wilcox, C. S. (2003) Effects of ANG II type 1 and 2 receptors on oxidative stress, renal NADPH oxidase, and SOD expression. *Am J Physiol Regul Integr Comp Physiol* **285**, R117-124.
- Chakrabarty, A., Blacklock, A., Svojanovsky, S. and Smith, P. G. (2008) Estrogen elicits dorsal root ganglion axon sprouting via a renin-angiotensin system. *Endocrinology* **149**, 3452-3460.
- Chakrabarty, A., Liao, Z., Mu, Y. and Smith, P. G. (2018) Inflammatory Renin-Angiotensin System Disruption Attenuates Sensory Hyperinnervation and Mechanical Hypersensitivity in a Rat Model of Provoked Vestibulodynia. *J Pain* **19**, 264-277.
- Chakrabarty, A., Liao, Z. and Smith, P. G. (2013) Angiotensin II receptor type 2 activation is required for cutaneous sensory hyperinnervation and hypersensitivity in a rat hind paw model of inflammatory pain. *J Pain* **14**, 1053-1065.
- Delree, P., Leprince, P., Schoenen, J. and Moonen, G. (1989) Purification and culture of adult rat dorsal root ganglia neurons. *J Neurosci Res* **23**, 198-206.
- Djoughri, L., Fang, X., Koutsikou, S. and Lawson, S. N. (2012) Partial nerve injury induces electrophysiological changes in conducting (uninjured) nociceptive and nonnociceptive DRG neurons: Possible relationships to aspects of peripheral neuropathic pain and paresthesias. *Pain* **153**, 1824-1836.
- Djoughri, L., Koutsikou, S., Fang, X., McMullan, S. and Lawson, S. N. (2006) Spontaneous pain, both neuropathic and inflammatory, is related to frequency of spontaneous firing in intact C-fiber nociceptors. *J Neurosci* **26**, 1281-1292.
- Djoughri, L. and Lawson, S. N. (2004) Abeta-fiber nociceptive primary afferent neurons: a review of incidence and properties in relation to other afferent A-fiber neurons in mammals. *Brain Res Brain Res Rev* **46**, 131-145.
- Dolley-Hitze, T., Jouan, F., Martin, B. et al. (2010) Angiotensin-2 receptors (AT1-R and AT2-R), new prognostic factors for renal clear-cell carcinoma? *Br J Cancer* **103**, 1698-1705.
- Dubin, A. E. and Patapoutian, A. (2010) Nociceptors: the sensors of the pain pathway. *J Clin Invest* **120**, 3760-3772.
- Esteban, V., Lorenzo, O., Ruperez, M. et al. (2004) Angiotensin II, via AT1 and AT2 receptors and NF-kappaB pathway, regulates the inflammatory response in unilateral ureteral obstruction. *J Am Soc Nephrol* **15**, 1514-1529.
- Fang, X., Djoughri, L., McMullan, S., Berry, C., Okuse, K., Waxman, S. G. and Lawson, S. N. (2005a) trkA is expressed in nociceptive neurons and influences electrophysiological properties via Nav1.8 expression in rapidly conducting nociceptors. *J Neurosci* **25**, 4868-4878.

- Fang, X., Djouhri, L., McMullan, S., Berry, C., Waxman, S. G., Okuse, K. and Lawson, S. N. (2006) Intense isolectin-B4 binding in rat dorsal root ganglion neurons distinguishes C-fiber nociceptors with broad action potentials and high Nav1.9 expression. *J Neurosci* **26**, 7281-7292.
- Fang, X., McMullan, S., Lawson, S. N. and Djouhri, L. (2005b) Electrophysiological differences between nociceptive and non-nociceptive dorsal root ganglion neurones in the rat in vivo. *J Physiol* **565**, 927-943.
- Gibson, S. J., Polak, J. M., Bloom, S. R. et al. (1984) Calcitonin gene-related peptide immunoreactivity in the spinal cord of man and of eight other species. *J Neurosci* **4**, 3101-3111.
- Goodman, S. L. (2018) The path to VICTORY - a beginner's guide to success using commercial research antibodies. *J Cell Sci* **131**.
- Guimond, M. O. and Gallo-Payet, N. (2012) How does angiotensin AT(2) receptor activation help neuronal differentiation and improve neuronal pathological situations? *Front Endocrinol (Lausanne)* **3**, 164.
- Hafko, R., Villapol, S., Nostramo, R., Symes, A., Sabban, E. L., Inagami, T. and Saavedra, J. M. (2013) Commercially available angiotensin II At(2) receptor antibodies are nonspecific. *PLoS One* **8**, e69234.
- Hashikawa-Hobara, N., Hashikawa, N., Inoue, Y., Sanda, H., Zamami, Y., Takatori, S. and Kawasaki, H. (2012) Candesartan cilexetil improves angiotensin II type 2 receptor-mediated neurite outgrowth via the PI3K-Akt pathway in fructose-induced insulin-resistant rats. *Diabetes* **61**, 925-932.
- Haskins, W., Benitez, S., Mercado, J. M. and Acosta, C. G. (2017) Cutaneous inflammation regulates THK1 expression in small C-like nociceptor dorsal root ganglion neurons. *Mol Cell Neurosci* **83**, 13-26.
- Hendrix, S. and Peters, E. M. (2007) Neuronal plasticity and neuroregeneration in the skin -- the role of inflammation. *J Neuroimmunol* **184**, 113-126.
- Iwasaki, Y., Ichikawa, Y., Igarashi, O., Kinoshita, M. and Ikeda, K. (2002) Trophic effect of olmesartan, a novel AT1R antagonist, on spinal motor neurons in vitro and in vivo. *Neurol Res* **24**, 468-472.
- Johren, O., Inagami, T. and Saavedra, J. M. (1995) AT1A, AT1B, and AT2 angiotensin II receptor subtype gene expression in rat brain. *Neuroreport* **6**, 2549-2552.
- Jones, E. S., Vinh, A., McCarthy, C. A., Gaspari, T. A. and Widdop, R. E. (2008) AT2 receptors: functional relevance in cardiovascular disease. *Pharmacol Ther* **120**, 292-316.
- Joseph, E. K. and Levine, J. D. (2010) Hyperalgesic priming is restricted to isolectin B4-positive nociceptors. *Neuroscience* **169**, 431-435.
- Kamber, M., Papalazarou, V., Rouni, G., Papageorgopoulou, E., Papalois, A. and Kostourou, V. (2015) Angiotensin II inhibitor facilitates epidermal wound regeneration in diabetic mice. *Front Physiol* **6**, 170.
- Kim, J. and Shin, W. (2014) How to do random allocation (randomization). *Clin Orthop Surg* **6**, 103-109.
- Koga, H., Yang, H., Haxhija, E. Q. and Teitelbaum, D. H. (2008) The role of angiotensin II type 1a receptor on intestinal epithelial cells following small bowel resection in a mouse model. *Pediatr Surg Int* **24**, 1279-1286.
- Kunda, P. E., Cavicchia, J. C. and Acosta, C. G. (2014) Lipopolysaccharides and trophic factors regulate the LPS receptor complex in nodose and trigeminal neurons. *Neuroscience* **280**, 60-72.
- Laflamme, L., Gasparo, M., Gallo, J. M., Payet, M. D. and Gallo-Payet, N. (1996) Angiotensin II induction of neurite outgrowth by AT2 receptors in NG108-15 cells. Effect counteracted by the AT1 receptors. *J Biol Chem* **271**, 22729-22735.
- Laitinen, L. (1987) Griffonia simplicifolia lectins bind specifically to endothelial cells and some epithelial cells in mouse tissues. *Histochem J* **19**, 225-234.
- Lawson, S. N. (2002) Phenotype and Function of Somatic Primary Afferent Nociceptive Neurones with C-, Adelta- or Alpha/beta-Fibres. *Exp Physiol* **87**, 239-244.

- Lawson, S. N., McCarthy, P. W. and Prabhakar, E. (1996) Electrophysiological properties of neurones with CGRP-like immunoreactivity in rat dorsal root ganglia. *J Comp Neurol* **365**, 355-366.
- Leiguarda, C., Coronel, M. F., Montaner, A. D., Villar, M. J. and Brumovsky, P. R. (2018) Long-lasting ameliorating effects of the oligodeoxynucleotide IMT504 on mechanical allodynia and hindpaw edema in rats with chronic hindpaw inflammation. *Neurosci Lett* **666**, 17-23.
- Lenkei, Z., Palkovits, M., Corvol, P. and Llorens-Cortes, C. (1997) Expression of angiotensin type-1 (AT1) and type-2 (AT2) receptor mRNAs in the adult rat brain: a functional neuroanatomical review. *Front Neuroendocrinol* **18**, 383-439.
- Li, J., Culman, J., Hortnagl, H. et al. (2005) Angiotensin AT2 receptor protects against cerebral ischemia-induced neuronal injury. *FASEB J* **19**, 617-619.
- Ma, W. and Quirion, R. (2014) Targeting cell surface trafficking of pain-facilitating receptors to treat chronic pain conditions. *Expert Opin Ther Targets* **18**, 459-472.
- Macova, M., Armando, I., Zhou, J., Baiardi, G., Tyurmin, D., Larrayoz-Roldan, I. M. and Saavedra, J. M. (2008) Estrogen reduces aldosterone, upregulates adrenal angiotensin II AT2 receptors and normalizes adrenomedullary Fra-2 in ovariectomized rats. *Neuroendocrinology* **88**, 276-286.
- Marion, E., Song, O. R., Christophe, T. et al. (2014) Mycobacterial toxin induces analgesia in buruli ulcer by targeting the angiotensin pathways. *Cell* **157**, 1565-1576.
- Marques-Lopes, J., Pinto, M., Pinho, D., Morato, M., Patinha, D., Albino-Teixeira, A. and Tavares, I. (2009) Microinjection of angiotensin II in the caudal ventrolateral medulla induces hyperalgesia. *Neuroscience* **158**, 1301-1310.
- Marsh, B., Acosta, C., Djouhri, L. and Lawson, S. N. (2012) Leak K(+) channel mRNAs in dorsal root ganglia: relation to inflammation and spontaneous pain behaviour. *Mol Cell Neurosci* **49**, 375-386.
- Matavelli, L. C. and Siragy, H. M. (2015) AT2 receptor activities and pathophysiological implications. *J Cardiovasc Pharmacol* **65**, 226-232.
- Namsolleck, P., Boato, F., Schwengel, K. et al. (2013) AT2-receptor stimulation enhances axonal plasticity after spinal cord injury by upregulating BDNF expression. *Neurobiol Dis* **51**, 177-191.
- Parekh, A., Campbell, A. J., Djouhri, L., Fang, X., McMullan, S., Berry, C., Acosta, C. and Lawson, S. N. (2010) Immunostaining for the alpha3 isoform of the Na⁺/K⁺-ATPase is selective for functionally identified muscle spindle afferents in vivo. *J Physiol* **588**, 4131-4143.
- Patil, J., Schwab, A., Nussberger, J., Schaffner, T., Saavedra, J. M. and Imboden, H. (2010) Intraneuronal angiotensinergic system in rat and human dorsal root ganglia. *Regul Pept* **162**, 90-98.
- Pavel, J., Oroszova, Z., Hricova, L. and Lukacova, N. (2013) Effect of subpressor dose of angiotensin II on pain-related behavior in relation with neuronal injury and activation of satellite glial cells in the rat dorsal root ganglia. *Cell Mol Neurobiol* **33**, 681-688.
- Pavel, J., Tang, H., Brimijoin, S., Moughamian, A., Nishioku, T., Benicky, J. and Saavedra, J. M. (2008) Expression and transport of Angiotensin II AT1 receptors in spinal cord, dorsal root ganglia and sciatic nerve of the rat. *Brain Res* **1246**, 111-122.
- Pinho-Ribeiro, F. A., Verri, W. A., Jr. and Chiu, I. M. (2017) Nociceptor Sensory Neuron-Immune Interactions in Pain and Inflammation. *Trends Immunol* **38**, 5-19.
- Ranjbar, R., Shafiee, M., Hesari, A., Ferns, G. A., Ghasemi, F. and Avan, A. (2019) The potential therapeutic use of renin-angiotensin system inhibitors in the treatment of inflammatory diseases. *J Cell Physiol* **234**, 2277-2295.
- Rice, A. S. C., Dworkin, R. H., McCarthy, T. D. et al. (2014) EMA401, an orally administered highly selective angiotensin II type 2 receptor antagonist, as a novel treatment for postherpetic neuralgia: a randomised, double-blind, placebo-controlled phase 2 clinical trial. *Lancet* **383**, 1637-1647.

- Ruiz-Ortega, M., Lorenzo, O., Ruperez, M., Esteban, V., Suzuki, Y., Mezzano, S., Plaza, J. J. and Egido, J. (2001) Role of the renin-angiotensin system in vascular diseases: expanding the field. *Hypertension* **38**, 1382-1387.
- Sanchez, S. I., Seltzer, A. M., Fuentes, L. B., Forneris, M. L. and Ciuffo, G. M. (2008) Inhibition of Angiotensin II receptors during pregnancy induces malformations in developing rat kidney. *Eur J Pharmacol* **588**, 114-123.
- Sharma, H., Ji, E., Yap, P., Vilimas, P., Kyloh, M., Spencer, N. J., Haberberger, R. V. and Barry, C. M. (2018) Innervation Changes Induced by Inflammation in the Murine Vagina. *Neuroscience* **372**, 16-26.
- Shepherd, A. J., Copits, B. A., Mickle, A. D. et al. (2018) Angiotensin II Triggers Peripheral Macrophage-to-Sensory Neuron Redox Crosstalk to Elicit Pain. *J Neurosci* **38**, 7032-7057.
- Shepherd, A. J. and Mohapatra, D. P. (2018) Attenuation of Unevoked Mechanical and Cold Pain Hypersensitivities Associated With Experimental Neuropathy in Mice by Angiotensin II Type-2 Receptor Antagonism. *Anesth Analg*.
- Shim, B., Kim, D. W., Kim, B. H., Nam, T. S., Leem, J. W. and Chung, J. M. (2005) Mechanical and heat sensitization of cutaneous nociceptors in rats with experimental peripheral neuropathy. *Neuroscience* **132**, 193-201.
- Smith, G. R. and Missailidis, S. (2004) Cancer, inflammation and the AT1 and AT2 receptors. *J Inflamm (Lond)* **1**, 3.
- Smith, M. T. and Muralidharan, A. (2015) Targeting angiotensin II type 2 receptor pathways to treat neuropathic pain and inflammatory pain. *Expert Opin Ther Targets* **19**, 25-35.
- Smith, M. T., Wyse, B. D. and Edwards, S. R. (2013) Small molecule angiotensin II type 2 receptor (AT(2)R) antagonists as novel analgesics for neuropathic pain: comparative pharmacokinetics, radioligand binding, and efficacy in rats. *Pain Med* **14**, 692-705.
- Stefanini, M., De Martino, C. and Zamboni, L. (1967) Fixation of ejaculated spermatozoa for electron microscopy. *Nature* **216**, 173-174.
- Suzuki, Y., Ruiz-Ortega, M., Lorenzo, O., Ruperez, M., Esteban, V. and Egido, J. (2003) Inflammation and angiotensin II. *Int J Biochem Cell Biol* **35**, 881-900.
- Tarpley, J. W., Kohler, M. G. and Martin, W. J. (2004) The behavioral and neuroanatomical effects of IB4-saporin treatment in rat models of nociceptive and neuropathic pain. *Brain Res* **1029**, 65-76.
- Tashima, R., Koga, K., Sekine, M. et al. (2018) Optogenetic Activation of Non-Nociceptive Abeta Fibers Induces Neuropathic Pain-Like Sensory and Emotional Behaviors after Nerve Injury in Rats. *eNeuro* **5**, eN-NWR-0450-0417.
- Wolf, G., Wenzel, U., Burns, K. D., Harris, R. C., Stahl, R. A. and Thaiss, F. (2002) Angiotensin II activates nuclear transcription factor-kappaB through AT1 and AT2 receptors. *Kidney Int* **61**, 1986-1995.
- Yang, H., Shaw, G. and Raizada, M. K. (2002) ANG II stimulation of neuritogenesis involves protein kinase B in brain neurons. *Am J Physiol Regul Integr Comp Physiol* **283**, R107-114.
- Zwick, M., Davis, B. M., Woodbury, C. J., Burkett, J. N., Koerber, H. R., Simpson, J. F. and Albers, K. M. (2002) Glial cell line-derived neurotrophic factor is a survival factor for isolectin B4-positive, but not vanilloid receptor 1-positive, neurons in the mouse. *J Neurosci* **22**, 4057-4065.

Figure legends

Figure 1: Time-line diagram of the *in vivo* pharmacological experiments

18 adult female rats were randomly allocated (using simple sequence randomization) to 3 experimental groups of 6 rats each. The control group received normal drinking water (NDW) during 28 days; the second group was given an effective oral dosage of 20 mg/kg Losartan to inhibit AT1R. The third group was treated as the second with the administration of a daily dose of 1 mg/kg PD123319 (PD) from days 25 to 28. This allowed us to examine the effect of antagonizing AT1R and AT2R at the same time. On day 28, all rats received a single intradermal injection of CFA in the hindpaw and were all culled 24h later for tissue harvesting.

Figure 2: Phenotypic characterization of normal L5 DRG neurons expressing AT2R and their correlation with AT1R.

(A-B) Representative photomicrographs of ABC/DAB staining of AT2R and AT1R. Black arrows: AT2R+ neurons. Asterisks: AT2R- large neurons. Plots of either AT2R (n=117 neurons) or AT1R (n=223 neurons) cytoplasmic %intensities versus cross-sectional areas (in μm^2). Spearman's correlation values (r_s) and level of significance are indicated in each plot. Horizontal dotted lines mark the limit between negatively stained (intensity <20%) and positively stained neurons ($\geq 20\%$). **(C)** Co-localization of AT2R and AT1R. AT2R+/AT1R+ neurons are indicated by white arrows. The bar graph shows the proportions of AT2R+ neurons that are also AT1R+ and vice versa. **(D)** Triple immunofluorescence for AT2R, IB4-binding and trkA. There are AT2R+ neurons positively stained against trkA, IB4 or both phenotypic markers. **(E)** Plots show that cytoplasmic %intensities of AT2R significantly and positively correlate with IB4 but not with trkA (n=118 neurons). In the trkA plot, dotted lines indicate 3 neuronal groups: negatively stained neurons (<20%), weakly trkA+ neurons (20-40% intensity) and strongly trkA+ (>40%). **(F)** Triple immunofluorescence confocal photomicrographs stained against AT2R, RT97 and trkA. The white arrow points to a possible A β -nociceptor. Significance is ***p<0.001.

Figure 3: Central and peripheral projections of AT2R+ peptidergic and non-peptidergic DRG neurons.

Double immunofluorescence for AT2R (red) and IB4-binding (green) in normal spinal cord (A), dorsal root (B), spinal nerve (C), sciatic nerve (D) and skin (E). There was a modest overlap in the lamina III inner (LIII) between AT2R and IB4. White arrows indicate co-localizations of AT2R with IB4-stained fibers. Arrowheads point to AT2R+ and IB4- fibers.

Asterisk in E corresponds to a nerve bundle. (F-H) Double immunofluorescence against AT2R (red) and Substance P (SP, green) in: spinal cord (F), dorsal root (G) and spinal nerve (H). There was a significant overlap in the lamina I (LI) and II outer (LIlo) between AT2R and SP. Most AT2R+ fibers were also stained for SP, as indicated by white arrows. Arrowheads indicate AT2R+ and SP- fibers.

Figure 4: Inflammatory soup increased AT2R but not AT1R expression in DRG neurons *in vitro*.

(A) Top: representative PCR blot showing the expression of AT2R mRNA in purified DRG cultures under three experimental conditions (No trophic factor or NTF, 10 ng/ml NGF and 20 ng/ml GDNF) with and without the addition for 24h of an Inflammatory Soup (IS). Adrenal gland tissue (Adr) was used as a positive control. Bottom: bar plot showing the ratio of AT2R to β -actin relative mRNA levels. Addition of the IS resulted in increased levels of AT2R mRNA in all experimental conditions. GDNF alone was also able to significantly increase AT2R mRNA. **(B)** Top: as in **(A)**, but for AT1R. Bottom: neither the addition of trophic factors nor the IS changed the amount of AT1R mRNA relative to β -actin. Bars to the left side of the blots indicate the ladder weight expressed in bp. Data from 3 separate cultures from 3 rats (n=3). Significance is as follows *p<0.05, #, **p<0.01.

Figure 5: One- and four-days Complete Freund's Adjuvant (CFA) affected AT2R expression in different subpopulations of DRG neurons

(A) and (C) Representative photomicrographs of ABC/DAB staining of AT2R in normal (not treated, N), contralateral (C) and ipsilateral (I) L5 DRG mid-sections after one **(A)** and four **(C)** days of CFA-induced cutaneous inflammation (CFA1 and CFA4). Black arrows: neurons with very weak or absent staining at the cell edge and a high concentration in the perinuclear region. **(B) and (D)** Bar plots of AT2R intensities at three sub-cellular regions (whole cytoplasm, cell edge and inner) in DRG neurons of N and CFA1-4 (C and I) rats. Each dot represents the average %intensity of numerous neurons belonging to a single rat. The plots show data from 5 untreated rats, 5 CFA1 and 5 CFA4 rats (a dot per rat) and the mean \pm SEM. At CFA1 only small neurons showed a significant increment in AT2R intensity at the edge and inner regions with no changes in medium neurons. At CFA4 medium size neurons showed a significant increment in AT2R intensity at the edge and inner regions while small neurons lacked any significant change. Significance is as follows *p<0.05 and **p<0.01.

Figure 6: Cutaneous inflammation increased AT1R expression only at CFA4 and in large L5 DRG neurons

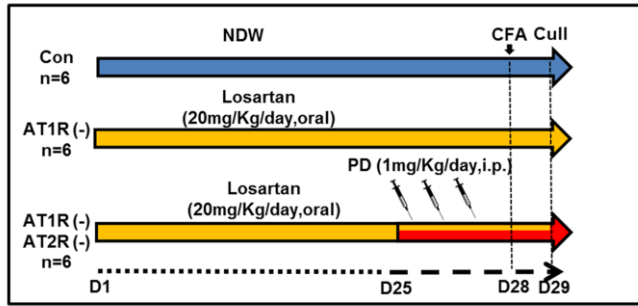
Bar plots of AT1R %intensities at whole cytoplasm, cell edge and inner at CFA1 (A) and CFA4 (B). Comparisons were made with normal DRGs (from untreated rats, N) and also between the contralateral (C) and ipsilateral (I) side of the animal. The plots show the mean±SEM from 5 untreated rats, 5 rats at CFA1 and 5 rats at CFA4. Each dot represents the average %intensity for a single animal. Notice that, unlike AT2R, CFA1 had no overall effect on AT1R expression. However, at CFA4 only large neurons underwent a significant elevation of AT1R expression, with no changes seen in small or medium size neurons. Significance is as follows *p<0.05 and **p<0.01.

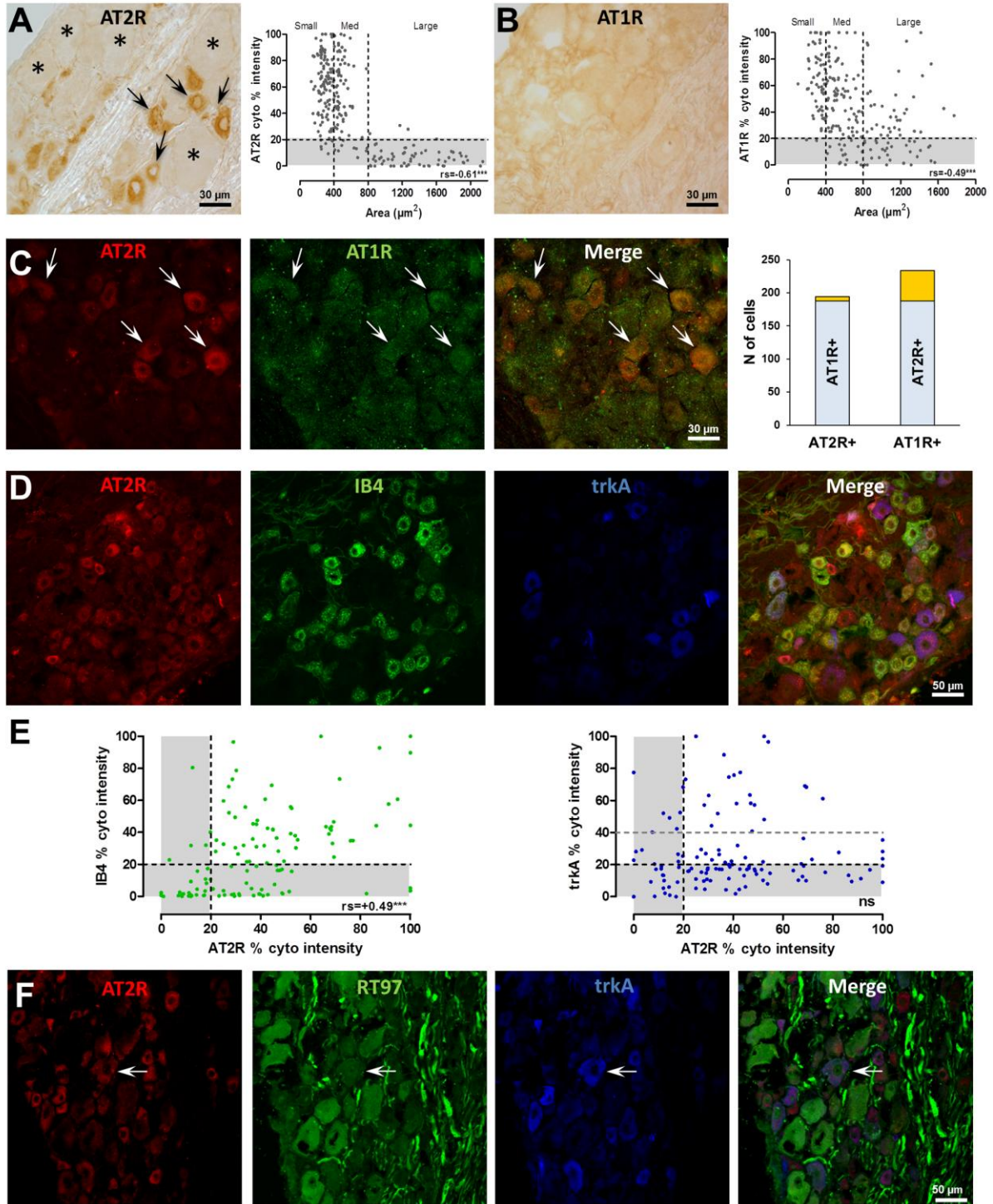
Figure 7: AT1R and AT2R contributed to the increase in neurite length induced by Ang-II in DRG neurons *in vitro*.

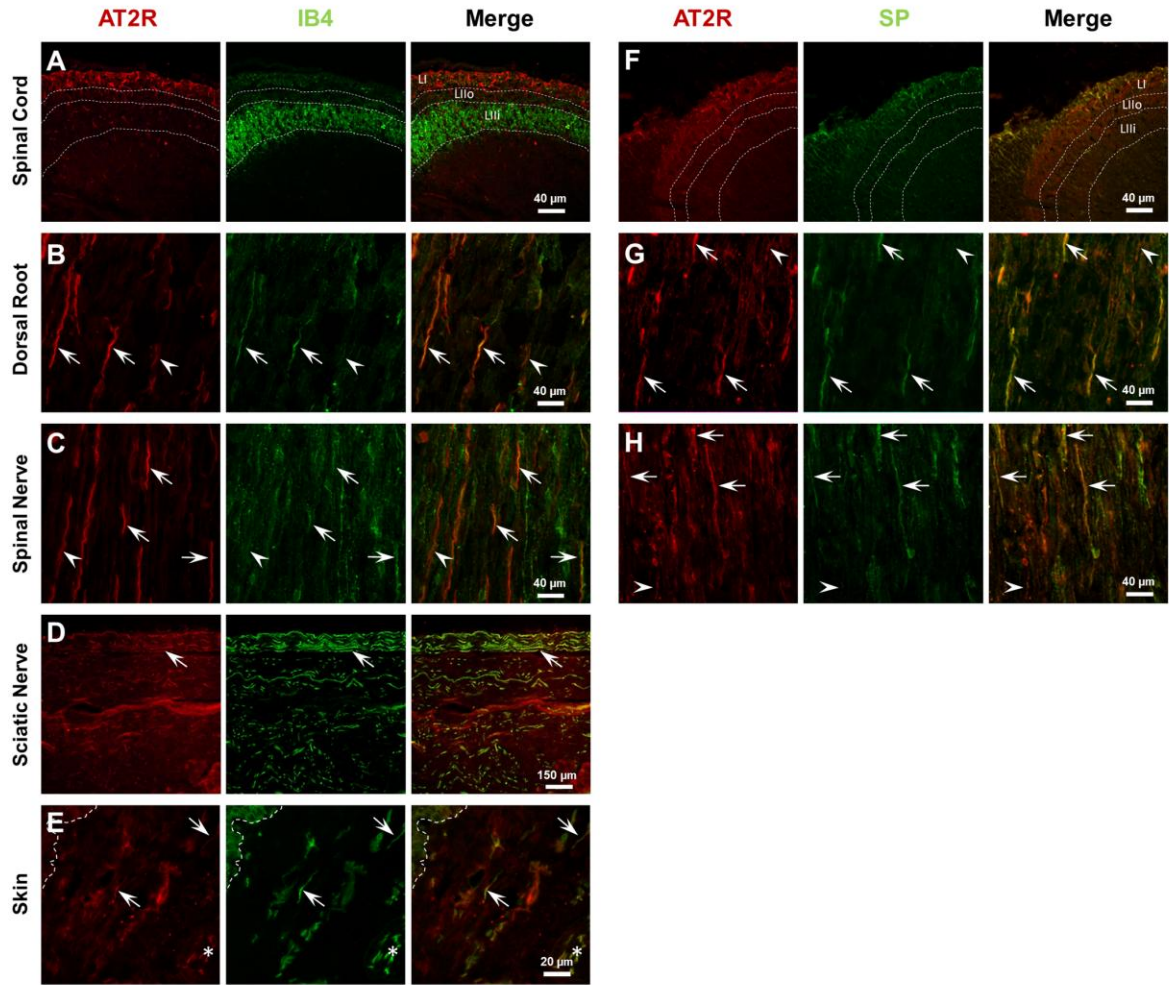
Representative confocal micrographs of all 6 experimental conditions are shown: no trophic factors (A), NGF (B), Ang-II (C), Ang-II+PD123319 (D), Ang-II+Azilsartan (E) and Ang-II+PD123319+Azilsartan (F). The far right column shows the masks generated to measure the total neurite length in each experimental condition. (G) Bar plot shows the neurite length (µm) per neuron in all conditions. Ang-II promoted neurite outgrowth in these neurons, an effect that was reverted by blocking AT1R with azilsartan and also by inhibiting AT2R with PD123319. Each dot represents the average neurite length measured in the neurons of 1 coverslip. Data from 3 separate cultures from 3 independent rats. Significance is as follows *p<0.05, **p<0.01 and ***p<0.001.

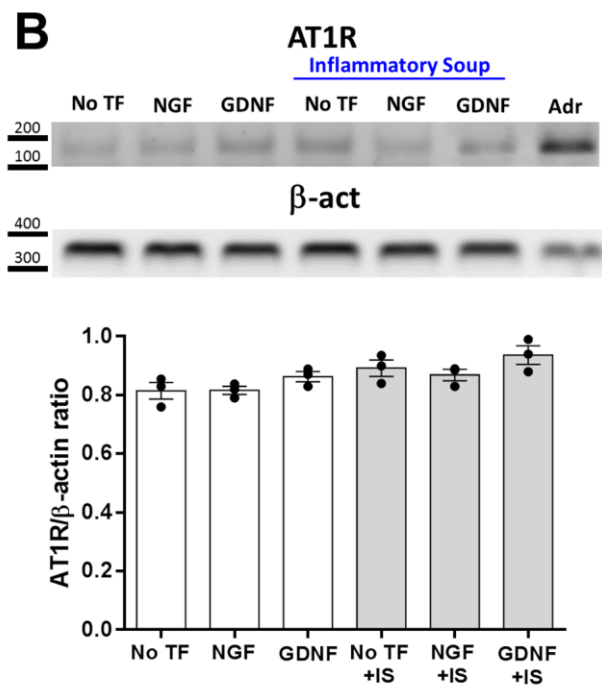
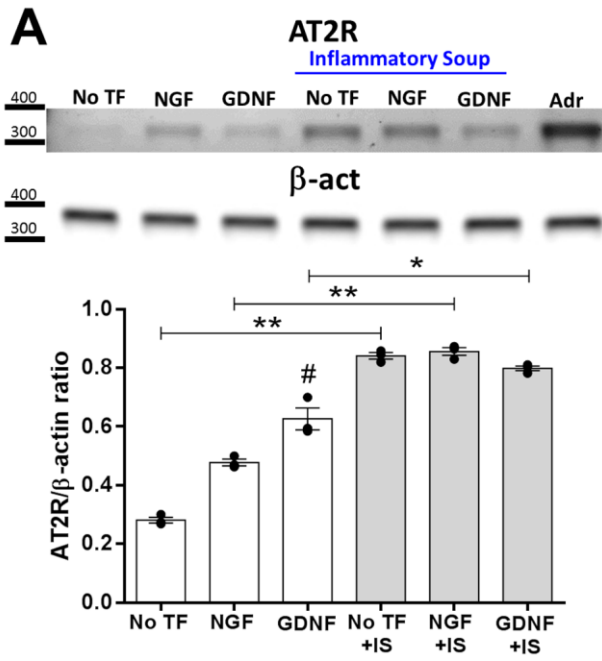
Figure 8: *In vivo* AT1R and AT2R antagonists altered the CFA-induced increment in neurite density of the hindpaw skin.

Representative photomicrographs of ipsilateral skin of the hindpaw with (A) RT97 and DAPI; (B) IB4-binding and β-TubIII; (C) CGRP and β-TubIII. Three experimental groups are shown: CFA1, CFA1 in rats pre-treated with oral losartan (CFA+Los) and CFA1 in rats pre-treated with oral losartan plus i.p. PD123319 for 3 days prior to CFA injection (CFA+Los+PD). Bar plots show the density of the visible nerve terminals for each marker in the contralateral and ipsilateral paw in the three experimental groups (n=6 rats per group). White arrows point to nerve terminals that were quantified. Dotted lines demarcate the limit between the epidermis (Epi) and the endodermis. Significance is as follows *p<0.05 and **p<0.01.

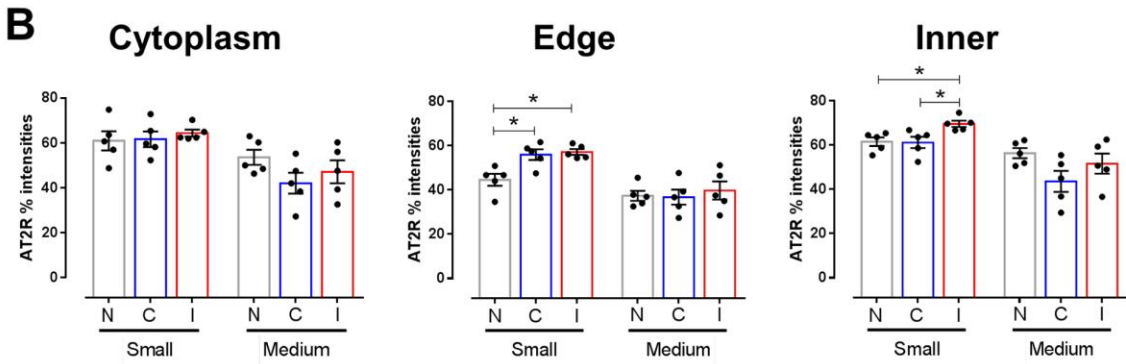
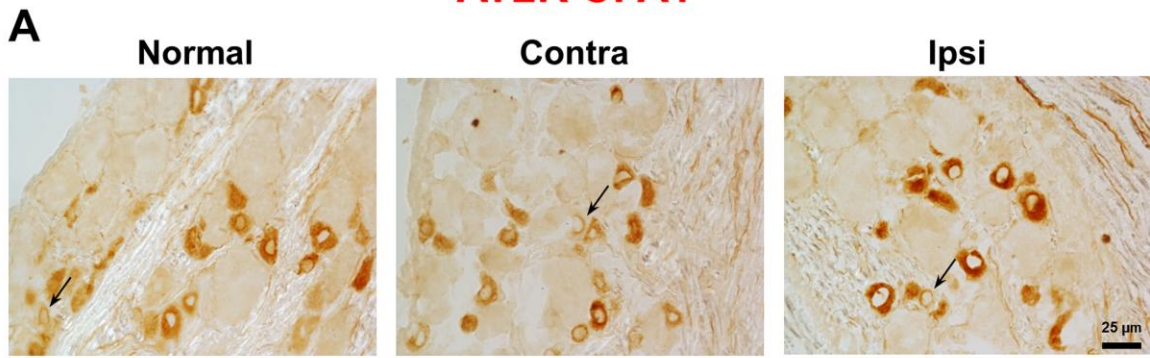




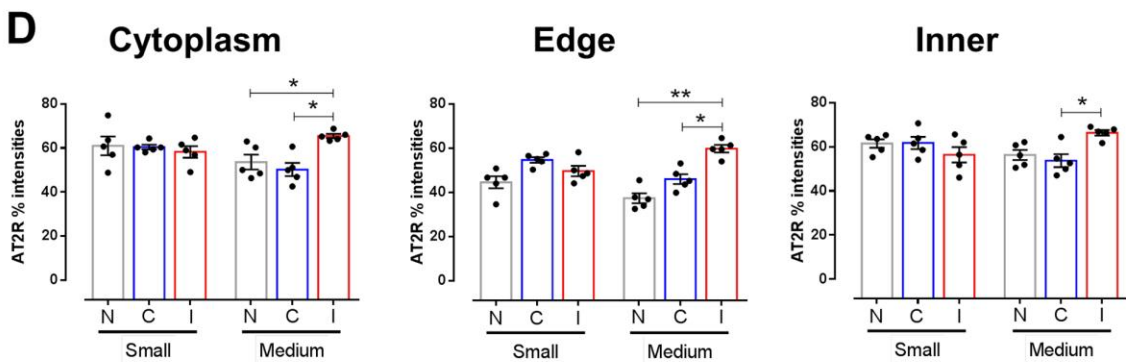


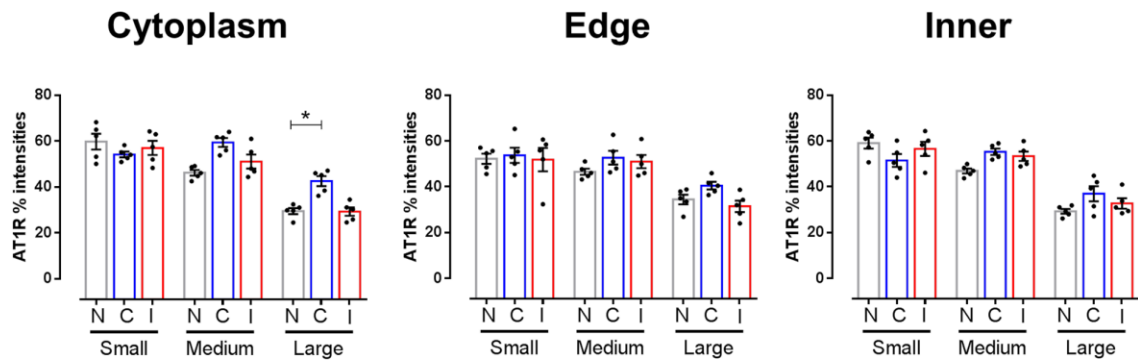


AT2R CFA1



AT2R CFA4



A**AT1R CFA1****B****AT1R CFA4**